Topics in Applied Physics
Volume 119

Topics in Applied Physics

Topics in Applied Physics is a well-established series of review books, each of which presents a comprehensive survey of a selected topic within the broad area of applied physics. Edited and written by leading research scientists in the field concerned, each volume contains review contributions covering the various aspects of the topic. Together these provide an overview of the state of the art in the respective field, extending from an introduction to the subject right up to the frontiers of contemporary research.

Topics in Applied Physics is addressed to all scientists at universities and in industry who wish to obtain an overview and to keep abreast of advances in applied physics. The series also provides easy but comprehensive access to the fields for newcomers starting research.

Contributions are specially commissioned. The Managing Editors are open to any suggestions for topics coming from the community of applied physicists no matter what the field and encourage prospective editors to approach them with ideas.

Managing Editor

Dr. Claus E. Ascheron

Springer-Verlag GmbH

Tiergartenstr. 17

69121 Heidelberg

Germany

Email:claus.ascheron@springer.com

Assistant Editor

Adelheid H. Duhm

Springer-Verlag GmbH

Tiergartenstr. 17

69121 Heidelberg

Germany

Email:adelheid.duhm@springer.com

David J. Lockwood · Lorenzo Pavesi (Eds.)

Silicon Photonics II

Components and Integration

With 196 Figures

Springer

Editors
Dr. David J. Lockwood
National Research Council of Canada
Institute for Microstructural Sciences
1200 Montreal Road
Bldg. M-50
Ottawa Ontario K1A 0R6
Canada
david.lockwood@nrc-cnrc.gc.ca

Prof. Lorenzo Pavesi
Università di Trento
Dipartimento di Fisica
Laboratorio Nanoscienze
Via Sommarive 14
38050 Povo
Italy
lorenzo.pavesi@unitn.it

ISSN 0303-4216 e-ISSN 1437-0859
ISBN 978-3-642-10505-0 e-ISBN 978-3-642-10506-7
DOI 10.1007/978-3-642-10506-7
Springer Heidelberg Dordrecht London New York

Library of Congress Control Number: 2004046611

Cover design: Integra Software Services Pvt. Ltd., Pondicherry

Printed on acid-free paper

Springer is part of Springer Science+Business Media (www.springer.com)

In memory of Ulrich Gösele (1949–2009), a pioneer and leading light of silicon nanotechnology.

Preface

Optoelectronics and photonics are playing an essential role in many aspects of daily life, including information and communication technologies, environmental and green technologies, mechanical and chemical sensing, consumer electronics, and biomedicine. So far, the use of optical components in communication systems has been mainly limited to direct replacement of electrical cables by optical cables. With the continual increase in link bit rates, optical cables are now replacing electrical cables for shorter and shorter interconnect lengths. Optoelectronic and photonic technologies are becoming less costly and more integrated, and there is currently an opportunity for optics to move "inside the box" and change the interconnect topology at all levels.

Currently, most optoelectronic devices are fabricated as discrete components. This approach is based on serial (e.g., step-by-step) fabrication and packaging, and it makes optoelectronic technology drastically different compared to microelectronics, where the domination of parallel fabrication made possible ultra-large-scale integration with the price of individual devices below $\$10^{-8}$. Also, discrete assembly reduces the optoelectronic system reliability and decreases the manufacturing yield. Additional complications arise due to materials issues: in microelectronics the major material is elemental Si, while traditional semiconductor materials for optoelectronics are III–V alloys with much more complex technological requirements. Finally, optical waveguides and waveguide based devices are very bulky compared to electron devices; thus, the densities of electron devices in integrated circuits are many orders of magnitude greater compared to that in integrated optoelectronic systems.

Silicon photonics, where photonics devices are fabricated by using silicon or silicon compatible materials and where the manufacturing is based on the available microelectronics infrastructure, is emerging as the technology that can face all these challenges. The first volume of this series of books on silicon photonics appeared in 2004. We stated then that "This book is aimed at presenting the fascinating picture of the state of-the-art in silicon photonics and providing perspectives on what can be expected in the near future." Many of the visionary concepts reported there have been surpassed by reality. Silicon photonics is booming and growing at an incredible pace with many breakthroughs appearing day by day. Speed, integration density, active components, logic, nonlinear optics, etc., are all surpassed frontiers, which

silicon photonics has continuously moved apart. At the beginning of the second decade of the new millennium, several devices enabled by silicon photonics are already on the market and new ones are emerging day by day.

Due to the broad nature and importance of the topic, as well as the rapid progress in this field, it is quite appropriate to publish this sequel to our first book on *Silicon Photonics* in the Springer Topics in Applied Physics Series. We envisaged this book as the second of a series of books on silicon photonics, i.e., we are willing to produce further books on this topic as the field develops.

The present book is focused on components and integration and opens with a Chapter by Yamada, which reviews the fundamental characteristics and basic applications of such waveguides. Some passive devices, such as branches and wavelength filters, and dynamic devices based on the thermo-optic effect or carrier plasma effect have been developed by using silicon photonic wire waveguides. These waveguides also offer an efficient media for nonlinear optical functions, such as wavelength conversion. Their optical polarization characteristics can be a serious obstacle to some practical applications, but such difficulties can be eliminated by using a monolithically integrated polarization diversity system. Chapter 2 by Xu explores further the problems associated with mode polarization in waveguides. This chapter reviews the characteristics of silicon-on-insulator ridge waveguide birefringence, as governed by the waveguide cross-section geometry, the cladding stress level, and cladding thickness. Typical stress levels in dielectric cladding films such as silicon dioxide and silicon nitride are such that the stress-induced birefringence is of comparable magnitude to the waveguide geometrical birefringence. Hence the total waveguide birefringence can be precisely controlled by counter balancing these two factors. The application of this technique for achieving polarization independence and polarization splitting in photonic components is described using passive and active tuning of the stress-induced birefringence. In Chapter 3 Roelkens and Van Thourhout elaborate on the use of diffraction gratings to achieve an efficient, compact, alignment-tolerant, polarization-independent, and broadband optical coupling between an optical fiber and optoelectronic components. An optical probe based on a diffraction grating integrated on the facet of a single-mode fiber is described that enables testing individual components in a silicon-on-insulator nanophotonic integrated circuit. Chapter 4 by Chang et al. tackles the difficult technical problem of providing on-chip light sources, which are a critical component for integrated silicon photonics but lag other photonic components in their level of development. Erbium is an optical dopant that can be employed as a viable means for on-chip light generation, which also has the advantage of being compatible with long-distance telecommunications transmission wavelengths. In this chapter, Er-doped silicon-rich silicon nitride and Er silicates are introduced as promising host materials for compact on-chip light sources. Germanium on silicon is an enabler of silicon photonics as well as high-speed CMOS electronics and recently germanium has played a significant role in integrating materials such as III–Vs on silicon. In Chapter 5 Ichikawa et al. describe an ultra-thin germanium buffer layer technology that has created entirely new fields for applications such as high-efficiency cost-effective tandem solar cells using silicon as the cell as well as the mechanical substrate. Such

solar cells have successfully reproduced their ideal external quantum efficiency and prove that it is possible to successfully integrate silicon and GaAs.

The remaining four chapters focus on system integration. First, Scandurra in Chapter 6 describes possible applications of silicon photonics to the system-on-chip (SoC) domain. The higher and higher integration density is becoming such that many issues arise when a SoC has to be integrated, and electrical limits of interconnect wires are a limiting factor for performance that could be overcome through the use of the optical interconnect. Today, many semiconductor industries are investigating such a novel field and a number of projects are currently in progress to demonstrate the feasibility of such a revolutionary on-chip communication system relying on both CMOS technology and photonics. Chapter 7 develops this concept further. Liao et al. highlight a recent demonstration of a silicon photonic integrated chip that is capable of transmitting data at an aggregate rate of 200 Gb/s. It is based on wavelength division multiplexing where an array of eight high-speed silicon optical modulators is monolithically integrated with a demultiplexer and a multiplexer. This demonstration represents a key milestone on the way to fabricating terabit per second transceiver chips to meet future demands. In Chapter 8 Pinguet et al. describe the intimate relationship between process, devices, and system design by examining the development of Luxtera's CMOS Photonics technology. They address the challenges of integrating optoeletronic elements, including germanium photodiodes, in a commercial CMOS process without significantly affecting the electronics performance and the manufacturability of the process. A complete monolithically integrated wavelength division multiplexed 40-Gbps transceiver chip is fabricated as an example of the application of their complete technology platform and to demonstrate its capabilities for optoelectronic integration. Lastly, Fedeli et al. in Chapter 9 address different ways to merge photonics devices on an electronic circuit with microelectronics tools on large size wafers. The preferred route is above-integrated-circuit fabrication, with two options ruled by thermal constraints. The high-temperature option is based on wafer bonding on an optical silicon-on-insulator module, and the low-temperature option relies on the heterogeneous integration of III–V devices.

Finally, we dedicate this book to the memory of Ulrich Gösele (1949–2009), our colleague who recently and prematurely passed away. He was among the first who initiated the field by discovering the quantum nature of porous silicon and the possibility of its use in optoelectronics. Moreover, he pioneered the technique of wafer bonding, which is nowadays a common practice to realize hybrid devices.

Ottawa, Canada — *David J. Lockwood*
Trento, Italy — *Lorenzo Pavesi*
June 2010

Contents

1 Silicon Photonic Wire Waveguides: Fundamentals and Applications . . 1
Koji Yamada
1.1 Introduction 1
1.2 Fundamental Design of Silicon Photonic Wire Waveguides 3
1.2.1 Guided Modes 3
1.2.2 Effect of Geometrical Errors and Birefringence 5
1.2.3 Propagation Loss and Radiation Loss in Bending 7
1.2.4 Coupling to External Fiber 8
1.3 Fundamental Propagation Performance 9
1.3.1 Fabrication 9
1.3.2 Propagation Performance 11
1.4 Simple Applications of Silicon Photonic Wire Waveguides 14
1.4.1 Passive Devices 14
1.4.2 Dynamic Devices 15
1.4.3 Nonlinear Functions 19
1.5 Polarization Manipulation 22
1.5.1 Polarization Splitter and Rotator 22
1.5.2 Polarization Diversity 25
1.6 Summary 26
References 26
Index 28

2 Polarization Control in Silicon Photonic Waveguide Components Using Cladding Stress Engineering 31
Dan-Xia Xu
2.1 Introduction 31
2.2 SOI Waveguides: General Considerations 33
2.2.1 Single-Mode Condition 34
2.2.2 Higher Order Mode Filtering 35
2.3 Waveguide Birefringence: Geometrical Effects 35
2.3.1 Waveguide Cross-Section 36
2.3.2 Scaling of the Geometrical Birefringence with Core Size . . . 38
2.3.3 Dispersion and Group Index Birefringence 39

2.4 Cladding Stress-Induced Birefringence: Theory and Modeling 40
2.4.1 Photoelastic Effect 40
2.4.2 Ordinary and Normalized Plane Strain Models 42
2.4.3 Cladding Stress-Induced Birefringence in Waveguides 45
2.4.4 Stress-Induced Mode Mismatch 49
2.4.5 Stress-Induced Effect on the Group Index Birefringence 49
2.4.6 Scaling of Stress-Induced Birefringence with the Core Size . 50
2.5 Cladding Stress Engineering: Applications 52
2.5.1 Polarization-Independent AWGs 52
2.5.2 Polarization-Independent Ring Resonator, Mach-Zehnder Interferometer, and Directional Coupler 54
2.5.3 Broadband Polarization Splitter in a Zero-Order AWG Configuration 58
2.5.4 Trimming of Birefringence in Passive Components 60
2.5.5 Phase Matching in Raman and Other Nonlinear Processes and Active Birefringence Tuning 62
2.5.6 Stress-Induced Pockels Electro-optic Effect in Silicon 63
2.6 Conclusions 64
References 65
Index 69

3 Interfacing Silicon Nanophotonic Integrated Circuits and Single-Mode Optical Fibers with Diffraction Gratings 71
Günther Roelkens and Dries Van Thourhout
3.1 Nanophotonic SOI Waveguide Circuits 71
3.2 Solutions to the Fiber-Chip Coupling Problem 72
3.3 Fundamentals of Fiber-Chip Diffraction Grating Couplers 73
3.4 High-Efficiency Fiber-Chip Grating Couplers 76
3.5 Multi-band Fiber-Chip Grating Couplers 80
3.6 Polarization Independent Fiber-Chip Coupling 83
3.7 Integration of Opto-electronic Components 88
3.8 Small Footprint Fiber-Chip Coupling Structures 89
3.9 Optical Probing of Nanophotonic Integrated Circuits 91
3.10 Conclusions 92
References 93
Appendix 94
Index 94

4 Development and Application of Er-Doped Silicon-Rich Silicon Nitrides and Er Silicates for On-Chip Light Sources 95
Jee Soo Chang, Kiseok Suh, Moon-Seung Yang, and Jung H. Shin
4.1 Introduction 95
4.1.1 Si Photonics and Light Sources 95
4.1.2 Er as an Optical Dopant 97
4.1.3 Silicon-Rich Silicon Nitride and Er Silicates 99

4.2 Er-Doped Silicon-Rich Silicon Nitride . . . 100
4.2.1 Experimental . . . 100
4.2.2 Results and Discussion . . . 101
4.2.3 Conclusion . . . 106
4.3 Er Silicates . . . 107
4.3.1 Experimental . . . 107
4.3.2 Results and Discussion . . . 108
4.4 Applications of Er-Doped SRSN: High-Q Microdisks . . . 118
4.4.1 Experimental . . . 118
4.4.2 Results and Discussion . . . 118
4.5 Conclusion . . . 127
References . . . 127
Index . . . 130

5 Germanium as a Material to Enable Silicon Photonics . . . 131
R. Ichikawa, S. Takita, Y. Ishikawa, and K. Wada
5.1 Introduction . . . 131
5.2 Material Design . . . 132
5.3 Device Design: Tandem Cells . . . 133
5.4 Materials and Device Characteristics: (Ge) Buffer on Si and Ge Solar Cell on Si . . . 137
5.5 Summary . . . 140
References . . . 140
Index . . . 141

6 Silicon Photonics: The System on Chip Perspective . . . 143
Alberto Scandurra
6.1 Introduction . . . 143
6.2 The System on Chip Paradigm . . . 144
6.3 On-Chip Communication . . . 146
6.3.1 On-Chip Bus . . . 147
6.3.2 Network on Chip . . . 148
6.4 SoC Integration Issues . . . 154
6.4.1 Electrical Interconnect Classification . . . 156
6.4.2 Electrical Interconnect Metrics . . . 157
6.5 On-Chip Optical Interconnect . . . 159
6.5.1 The PICMOS Project . . . 162
6.5.2 The WADIMOS Project . . . 164
6.6 Conclusion . . . 167
References . . . 168
Index . . . 168

7 High-Speed Photonic Integrated Chip on a Silicon Platform . . . 169
Ling Liao, Ansheng Liu, Hat Nguyen, Juthika Basak, Mario Paniccia, Yoel Chetrit, and Doron Rubin

7.1 Introduction . . . 169
7.2 Silicon Photonic Integrated Chip Design . . . 170
7.3 Integrated Chip Fabrication . . . 176
7.4 Device Performance . . . 177
7.4.1 High-Speed Performance of the Stand-Alone Silicon MZM . 177
7.4.2 Performance of the Standalone MUX/DEMUX . . . 179
7.4.3 DC Performance of an Integrated DEMUX, MZM, and MUX Chip . . . 180
7.4.4 High-Speed Performance of the Silicon PIC . . . 182
7.5 Conclusion . . . 184
References . . . 185
Index . . . 186

8 CMOS Photonics: A Platform for Optoelectronics Integration . . . 187
Thierry Pinguet, Steffen Gloeckner, Gianlorenzo Masini, and Attila Mekis
8.1 Introduction . . . 187
8.2 Enabling a CMOS Process for Photonics Integration . . . 188
8.2.1 Rationale for Front-End Integration . . . 189
8.2.2 SOI Substrate Design . . . 190
8.2.3 Waveguide Integration . . . 191
8.2.4 Photolithography . . . 192
8.2.5 Active Optical Device Integration . . . 193
8.2.6 Germanium Module . . . 194
8.2.7 Process Control and Monitoring . . . 197
8.2.8 Other Integration Elements . . . 198
8.3 Photonic Device Library . . . 199
8.3.1 Electronics Libraries: The Inspiration . . . 199
8.3.2 Library Hierarchy and Design Flow . . . 199
8.3.3 Device Concepts . . . 200
8.3.4 Design Selection: The Design-of-Experiment Approach . . . 203
8.3.5 The Role of Process Variability in Design Selection . . . 205
8.3.6 Design Verification and Device Models . . . 206
8.4 Design and Testing Infrastructure: The Tools of Success . . . 206
8.4.1 Wafer-Scale Optoelectronic Testing . . . 206
8.4.2 Design Automation Tools . . . 207
8.5 Example of CMOS Photonic System . . . 209
8.6 Conclusions . . . 214
References . . . 215
Index . . . 216

9 Photonics and Electronics Integration . . . 217
J.-M. Fedeli, B. Ben Bakir, L. Grenouillet, D. Marris-Morini, and L.Vivien
9.1 Introduction . . . 217
9.2 Ways to Integrate Photonics Devices on an Electronic Wafer . . . 218

9.2.1 Above IC Fabrication 219
9.2.2 Combined Fabrication 222
9.3 Back-Side Fabrication 223
9.4 Passive Photonic Circuitry 224
9.4.1 Guided Structures 224
9.4.2 Amorphous Silicon Waveguide Fabrication 226
9.4.3 Optical Couplers 227
9.4.4 Efficient and Polarization Insensitive In-Plane Fiber Couplers 229
9.4.5 Silicon-Based Optical Modulator 231
9.5 Germanium Waveguide Photodetectors 234
9.6 Laser Fabrication on 200 mm Wafer 237
9.6.1 Die to Wafer Bonding of III–V Semiconductor on Silicon . . 237
9.6.2 Design and Fabrication of InP Lasers with Microelectronics Tools 239
9.7 Conclusion 244
References 244
Index 248

Index 251

Chapter 1
Silicon Photonic Wire Waveguides: Fundamentals and Applications

Koji Yamada

Abstract This chapter reviews the fundamental characteristics and basic applications of the silicon photonic wire waveguide. Thanks to its ultra-small geometrical structures and compatibility with the silicon electronics, the silicon photonic wire waveguide provides us with a highly integrated platform for electronic–photonic convergence. For the practical achievement of this platform, however, we must search for ways to reduce the propagation loss and coupling loss to external fibers and overcome the polarization dependence. Progress has been made by applying state-of-the-art technologies specially tuned to the fabrication of nanometer structures, and the fundamental propagation performance has already become a practical standard. Some passive devices, such as branches and wavelength filters, and dynamic devices based on the thermo-optic effect or carrier plasma effect have been developed by using silicon photonic wire waveguides. These waveguides also offer an efficient media for nonlinear optical functions, such as wavelength conversion. Although polarization dependence remains a serious obstacle to the practical applications of these waveguides, waveguide-based polarization manipulation devices provide us with effective solutions, such as a polarization diversity system.

1.1 Introduction

In recent years, silicon photonics has attracted attention as an emerging technology for optical telecommunications and for optical interconnects in microelectronics. Based on highly sophisticated silicon semiconductor technology, silicon photonics would provide us with an inexpensive highly integrated electronic–photonic platform, in which ultra-compact photonic devices and electronic circuits are converged.

Similar to the existing silica-based or III–V semiconductor-based photonic systems, silicon photonics also requires an optical waveguide system. The waveguide

K. Yamada (✉)
NTT Microsystem Integration Laboratories, NTT Corporation,
Atsugi, 243-0198 Japan
e-mail: kyamada@aecl.ntt.co.jp

D.J. Lockwood, L. Pavesi (Eds.): *Silicon Photonics II*.
Topics in Applied Physics **119**, 1–29 (2011)
DOI 10.1007/978-3-642-10506-7_1

must have features that allow us to accommodate passive and dynamic photonic devices such as wavelength filters and modulators. The waveguide system must also be flexible enough to allow active functions, such as light emission and detection to be implemented. Of course, it should guarantee a sufficiently low propagation loss for constructing and integrating these photonic functions. Furthermore, for monolithic electronic–photonic convergence, the most important advantage of silicon photonics, the following requirements must be met:

(1) Waveguides should be constructed on silicon substrates or be constructed together with silicon electronic devices.
(2) Waveguide fabrication processes should not damage electronic devices.
(3) Waveguides should not be damaged by the processes for fabricating electronic devices.
(4) Waveguide materials must not be hazardous to silicon electronics.
(5) Geometrical criteria, such as the layout of photonic devices, should not interfere with the electronic circuit layout.

These requirements are very difficult to meet with conventional waveguide systems. For example, the fabrication process for conventional silica-based waveguide requires high temperatures exceeding 1,000 °C, which would seriously damage electronic devices. Moreover, silica-based waveguides have a large bending radius on the order of millimeters or even centimeters, making it impossible to integrate photonic circuits on an electronic chip, whose typical size is a few centimeters square. The III–V compound semiconductor-based waveguides and photonic devices have geometries smaller than those in the silica-based system; however, on a silicon substrate it is very difficult to epitaxially grow the high-quality III–V materials needed for the construction of practical photonic devices. Etching and other fabrication procedures are completely different from silicon processes. Moreover, III–V material contamination must be eliminated from silicon electronics. At present, it is therefore very difficult to introduce III–V compounds into silicon electronics. Polymer waveguides made of organic materials cause less damage to electronic devices. However, their use is limited to the uppermost layers formed after the electronic circuits are completed or to other regions separated from the electronic devices because they cannot withstand the temperatures used in electronic device fabrication.

Recently, silicon oxynitride (SiON) and silicon nitride (Si_3N_4) waveguides have also been proposed as a compact waveguide system [1, 2]; however, these silicon nitride waveguides might be not suitable for electronic–photonic convergence for infrared light at wavelengths around 1,500 nm. Silicon nitride materials formed by low-temperature deposition methods generally contain N–H bond residues, which readily absorb infrared light at around 1,500 nm. A high-temperature (1,000 °C or more) annealing can reduce the absorption, but the high-temperature process is not compatible with electronic devices.

From the viewpoint of material, a silicon-based waveguide is obviously preferable for electronic photonic convergence. So far, several types of silicon waveguides have been proposed such as rib-type waveguides with core dimensions of a few micrometers [3, 4] and photonic wire waveguides with core dimensions of several

hundreds of nanometers [5–10]. The latter are especially promising for electronic–photonic convergence because their ultra-small core dimensions and micrometer bending sections match the dimensions of electronic circuits. The waveguides are constructed on silicon-on-insulator (SOI) substrates, where the uppermost SOI layer is used as the waveguide core so that there is no need to form the core material. The cladding material is a silica-based material formed by a low-temperature process such as plasma-enhanced chemical vapor deposition (PE–CVD) [11].

Besides the advantages of silicon photonic wire waveguides in electronic–photonic convergence, highly integrated ultra-compact photonic circuits based on photonic wire waveguides guarantee low power consumption and low packaging cost. Furthermore, the waveguides also offer advanced functionality through the use of its semiconductor characteristics of silicon.

1.2 Fundamental Design of Silicon Photonic Wire Waveguides

1.2.1 Guided Modes

A schematic of s silicon photonic wire waveguide is shown in Fig. 1.1a. The waveguide consist of a silicon core and silica-based cladding. The core dimension should be determined so that a single-mode condition is fulfilled. The single-mode condition is very important in constructing practical functional devices because whether or not we can implement a desired function depends on the fundamental guided mode. The core dimension of single-mode silicon photonic wire waveguides is significantly smaller than that of conventional single-mode silica waveguides. In the waveguide system consisting of a silicon core and silica claddings, the refractive

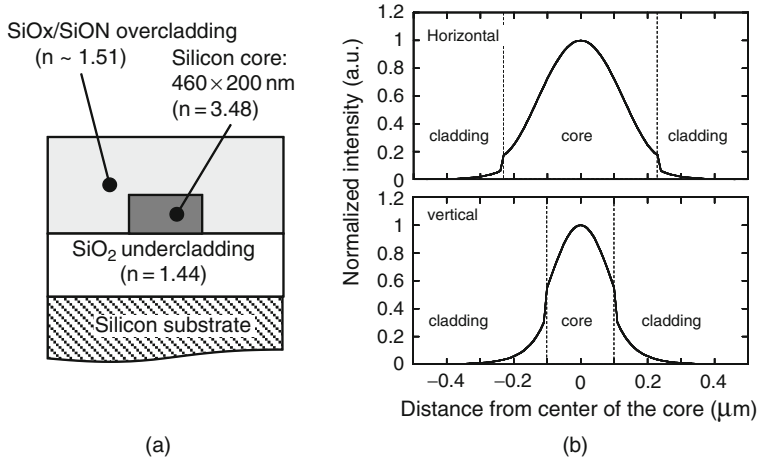

Fig. 1.1 (**a**) Cross-sectional structure and (**b**) optical intensity distribution of a typical silicon photonic wire waveguide

index contrast Δ between the core and cladding is as large as 40%, which allows a total internal reflection with a very large incident angle of 60°. This situation is similar to that in metallic rectangular waveguides, whose waveguide dimensions are smaller than or comparable to a half-wavelength of the guided electromagnetic waves. In silicon photonic wire waveguides, therefore, the core dimension that fulfills a single-mode condition should also be smaller than or comparable to a half-wavelength of a guided wave in silicon. Since the refractive index of silicon is about 3.5 for photon energies below the band-gap energy, the core dimension of a silicon photonic wire waveguide should be less than or comparable to 400 nm for 1,310∼1,550-nm telecommunications-band infrared light. Generally, the core shape is made flat along the substrate to reduce the etching depth in practical fabrications. In many cases, the height of the core is typically half of the width. Thus, a typical core geometry is a 400 × 200-nm^2 rectangle.

A detailed analysis of the guided modes can be performed by various numerical methods such as the finite difference method (FDM) [12], finite element method (FEM) [13], and film mode matching method (FMM) [14]. Figures 1.2a and b show calculated effective indices n_{eff} of guided modes for 1,550-nm infrared light in various core geometries. Calculations were performed by the FMM and the indices of silicon and silica were set at 3.477 and 1.444, respectively. The mode notations are taken from [15], in which E^x and E^y modes represent the transverse electric (TE)-like and transverse magnetic (TM)-like modes, respectively. As shown Fig. 1.2a for waveguides of 200-nm silicon thickness, single-mode conditions are fulfilled when the core width is less than 460 nm for TE-like guided modes in which the dominant electric field is parallel to the substrate. The mode field profile of the TE-like fundamental mode is shown in Fig. 1.1b for a 460 × 200-nm^2 core. For a TM-like mode in which the dominant electric field is perpendicular to the substrate,

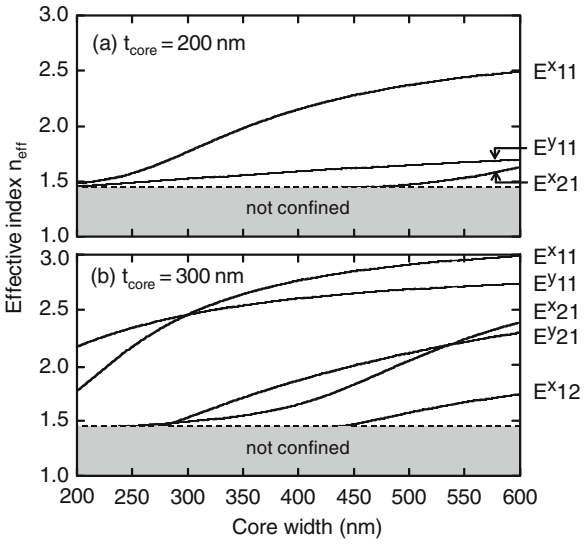

Fig. 1.2 Core width dependence of the effective indices of silicon photonic wire waveguides

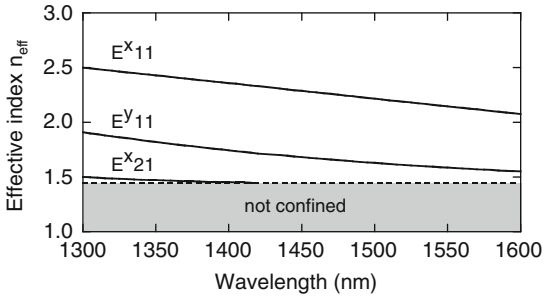

Fig. 1.3 Wavelength dependence of the effective indices of silicon photonic wire waveguides

the single-mode condition is fulfilled in a core larger than that for the TE-like mode. The effective indices of TE and TM fundamental modes show a large difference. In other words, the 200-nm-thick flat core produces a large polarization dependence. For waveguides with 300-nm-thick silicon as shown in Fig. 1.2b, core widths satisfying single-mode conditions are smaller than those for 200-nm-thick silicon. In a 300-nm^2 core, the refractive indices are identical for the TE and TM fundamental modes: that is, the polarization dependence can be eliminated.

Figure 1.3 shows the calculated wavelength dependence of the effective refractive indices for the waveguides with a 400×200-nm^2 core. Calculations were performed by the FMM and the material dispersions of refractive indices were considered. As shown in Fig. 1.3, the single-mode condition is violated in the wavelength region below 1,420 nm for the TE-like mode. For the 1,310-nm telecommunications wavelength band, therefore, a smaller core should be used for satisfying the single-mode condition.

1.2.2 Effect of Geometrical Errors and Birefringence

As shown in Fig. 1.2, the effective indices of silicon photonic wire waveguide are extremely sensitive to the core geometries. The group index n_g, which is an essential parameter in designing delay-based devices such as optical filters, is also affected significantly by the core geometry. Figures 1.4a and b show calculated group indices and their sensitivities to the core width $dn_g/n_g dw$. For TE-like modes, for which most of the photonic functions are designed, the sensitivities to the core width $dn_g/n_g dw$ are around 2×10^{-4} nm^{-1} for a 400×200-nm^2 core and much higher for a 300-nm^2 core. For wavelength filters for dense wavelength division multiplexing (DWDM), the group index should be controlled to on the order of 1×10^{-4} or less. The index restriction corresponds to a core width accuracy of 0.5 nm or less, which is essentially unattainable with current micro-fabrication technology. Fortunately, there are optimum geometries giving very low sensitivities to the core width. For example, 385×200-nm^2 and 325×300-nm^2 cores are robust against the errors in core width. Waveguides with a very wide core are also robust against the errors in core width. In an arrayed waveguide grating (AWG) filter, waveguides with 750×200-nm^2 cores are used to reduce phase errors due to the variation of

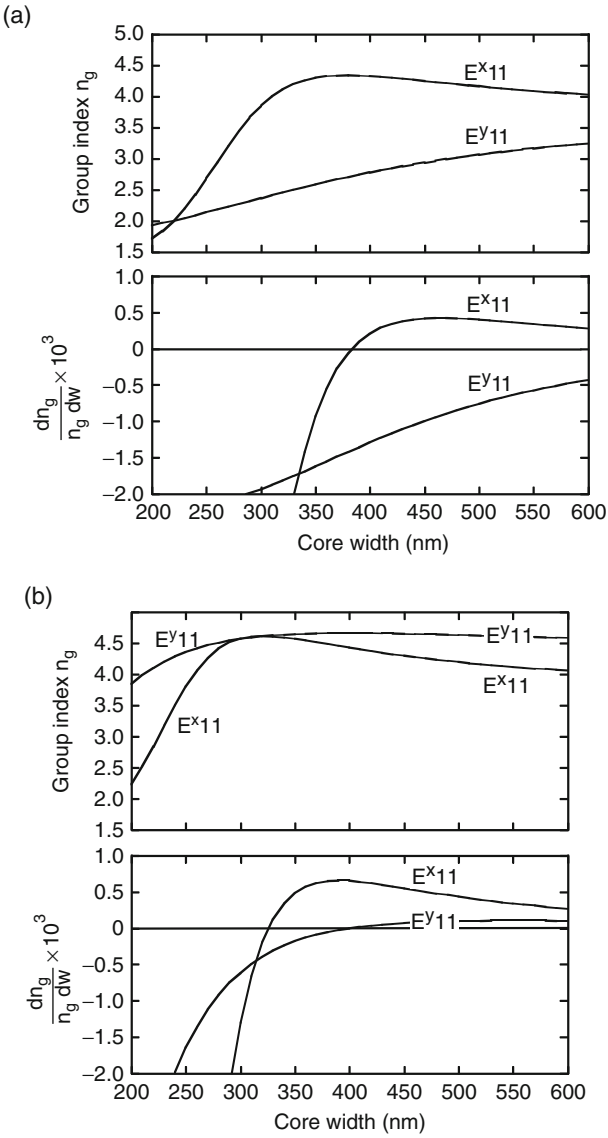

Fig. 1.4 (**a**) Core width dependence of the group indices and their derivatives for waveguides with 200-nm-thick cores (**b**) Core width dependence of the group indices and their derivatives for waveguides with 300-nm-thick cores

core width [16]. When we use such a wide-core waveguide, however, higher order modes stimulated in bending and other asymmetric structures become a concern.

Figure 1.4 also that the structural birefringence is incredibly large and that the problem of the polarization dependence in a silicon photonic wire waveguide is practically unsolvable. In a waveguide with a 400×200-nm^2 core, the group indices are 4.33 for the TE-like fundamental mode and 2.78 for the TM-like fundamental

mode. The difference in the group indices gives a polarization mode dispersion (PMD) of 51.7 ps/cm, which seriously limits the applicable bandwidth in high-speed data transmission. The polarization-dependent wavelength (PDλ) in delay-based filter devices, such as AWGs and ring resonators, would be incredibly large. A square core would not be a solution to this problem because the group index is very sensitive to the core geometry, as mentioned before. In other words, polarization diversity is necessary for eliminating the polarization dependence in photonic devices based on silicon photonic wire waveguides.

1.2.3 Propagation Loss and Radiation Loss in Bending

The intrinsic loss in undoped silicon is very low for the photon energies below the band gap (∼1.1 eV); therefore, the propagation loss of photonic wire waveguides is mainly determined by scattering due to surface roughness of the core. The effect of the surface roughness on the scattering loss in dielectric waveguides has been theoretically studied and formulated by Payne and Lacey [17]. The formula is represented by a complicated function characterized by a root-mean square roughness σ and the correlation length of the surface roughness structure l_c; the upper bound of the scattering loss α_{max}, as given in [18], is shown below.

$$\alpha_{max} = \frac{\sigma^2 \kappa}{k_0 d^4 n_1}, \tag{1.1}$$

where, k_0, d, and n_1 are wavevector of the light in vacuum, the half-width of the core, and effective index of a silicon slab with the same thickness as the core, respectively. The factor κ depends on the waveguide geometry and the statistical distribution (Gaussian, exponential, etc.) of the roughness, in which the correlation length l_c is included. According to [17], κ is on the order of unity for most practical waveguide geometries. Thus, the scattering loss is inversely proportional to the fourth power of d. In other words, it will seriously increase in photonic wire waveguides with an ultra-small core. A roughness of only 5 nm, for instance, would cause a 60-dB/cm scattering loss in a 400-nm-wide core made of a 200-nm-thick silicon slab whose effective index is 2.7. To achieve a practical scattering loss of a few decibels per centimeter, the surface roughness should be about 1 nm or less.

Radiation losses in the bending section can be calculated by applying cylindrical coordinates in numerical mode solvers. Figure 1.5 shows calculated radiation losses for a 90° bend in various waveguides. The calculations were performed by using a commercially available FMM mode solver [19]. As shown in this figure, the bending performance varies with polarization. For the TE-like mode in the waveguide with a 400×200-nm^2 core, the radiation loss is negligible even if the bending radius is as small as 2.5 μm. For the TM-like mode, however, a bending radius of over a few tens of micrometers is needed in order to achieve negligible radiation loss. The bending loss also varies with core dimensions. As shown in Fig. 1.5, for TE-like modes, a waveguide with a 300-nm^2 core requires a larger bending radius than a flat waveguide.

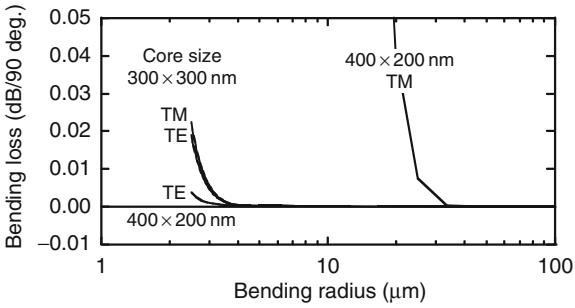

Fig. 1.5 Calculated radiation losses for a 90° bend in various waveguides

1.2.4 Coupling to External Fiber

Since a silicon photonic wire waveguide has a very small mode profile, spot-size conversion is essential for connecting it to external circuits such as single-mode optical fibers. A highly efficient spot size converter (SSC) with a silicon reverse adiabatic taper has already been proposed [20]. As shown in Fig. 1.6, it has a double-core structure consisting of a thin silicon taper and silica-based waveguides. In a typical design for 1,550-nm-wavelength infrared light, the tip of the taper should be ultimately reduced to less than 100 nm and the silica-based waveguide has a 3-μm^2 core with a 2.5% index contrast to the cladding. In such a double-core structure, light leaking from the silicon taper is captured by a silica-based waveguide, which guarantees efficient optical coupling to external optical fibers.

Figure 1.7 shows the calculated conversion efficiencies between a silicon photonic wire waveguide with a 400 × 200-nm^2 core and a silica-based waveguide with a 3-μm^2 core. As shown in this figure, a 200-μm-long taper with a 80-nm tip gives a conversion loss of around 0.1 dB for both polarizations. A shorter and thicker taper would give lower coupling efficiencies. Since the coupling loss between a silica-based waveguide with a 3-μm^2 core and a high-numerical-aperture (NA) fiber with a 4.3-μm mode field diameter is about 0.1 dB and the conversion loss between

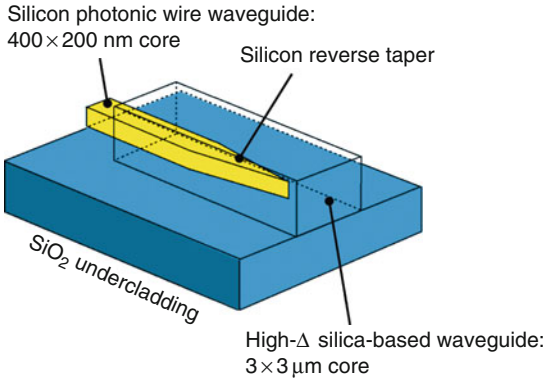

Fig. 1.6 Schematic of the spot size converter

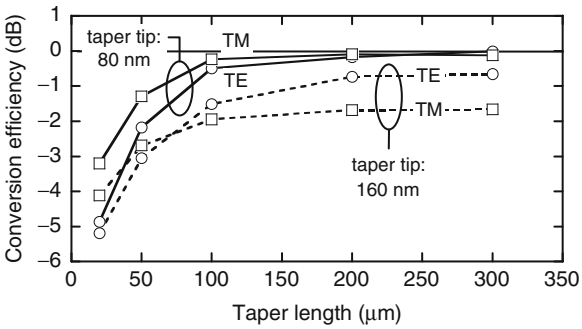

Fig. 1.7 Calculated conversion efficiencies in spot size converters with various geometries

the high-NA fiber and the ordinary single mode can be reduced to about 0.1 dB by applying a thermally expanded core (TEC) technology [21], a total coupling loss of less than 0.5 dB can be achieved between a photonic wire waveguide and a single-mode fiber.

A grating coupler input/output structure has also been proposed [22], for which the coupling efficiency between a photonic wire waveguide and an ordinary single-mode fiber is calculated to be −5 to −3 dB.

1.3 Fundamental Propagation Performance

1.3.1 Fabrication

Figure 1.8 shows a typical fabrication process for a Si-wire waveguide. First, a hard mask layer and resist mask layer are formed on a SOI substrate. The hard mask is used to improve the selectivity of Si etching and is often made of SiO_2. Next, waveguide patterns are defined by using electron beam (EB) lithography or excimer laser deep ultraviolet (DUV) lithography [9], which are capable of forming 100-nm patterns. Ordinarily, EB and DUV lithography technologies are used in the fabrication of electronic circuits where they are optimized for patterning of straight and intersecting line patterns. Therefore, no consideration has been given to curves and roughness in the pattern edges, which are important factors in fabricating low-loss optical waveguides. To reduce propagation losses of the waveguides, it is necessary to reduce the edge roughness to around 1 nm or less. This means that particular care must be taken in the data preparation for EB shots or DUV masks. Figure 1.9 shows an ultra-small ring resonator with and without special treatment for EB data preparation, where a drastic reduction in side-wall roughness is observed as a result of the special treatment [23]. The writing speed of the EB lithography must also be considered in practical fabrication. For practical purposes, it is probably necessary to use EB lithography with a variable-shaped beam.

After resist development and SiO_2 etching for a hard mask, the silicon core is formed by low-pressure plasma etching with an electron-cyclotron resonance (ECR) plasma or inductive coupled plasma. To ensure the edge roughness of the side walls

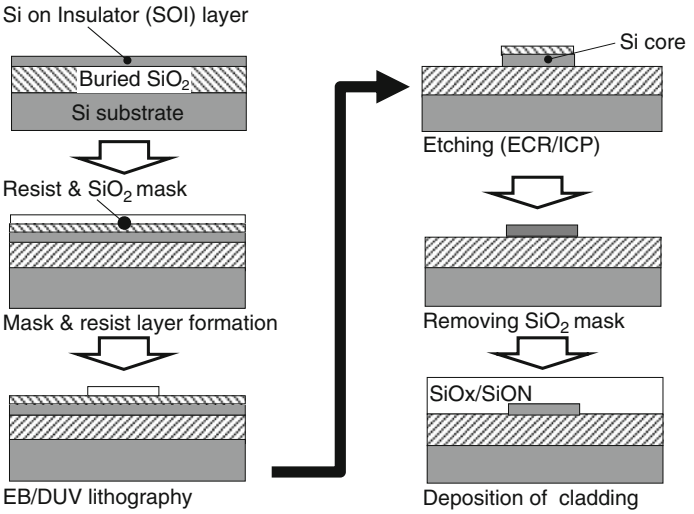

Fig. 1.8 Typical fabrication process of a silicon photonic wire waveguide

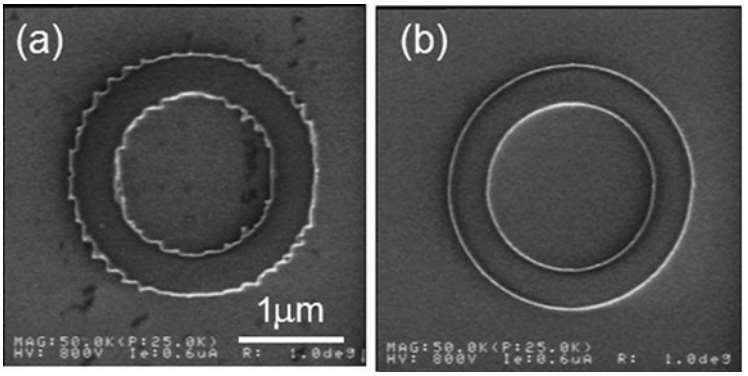

Fig. 1.9 SEM images of ring resonators (**a**) without and (**b**) with EB data optimizations

is at sub-nanometer levels, the plasma conditions and the selection of etching gases must be tuned for individual plasma equipment.

Finally, an overcladding layer is formed with a SiO_2-based material or polymer resin material. To avoid damaging the silicon layer, the cladding layers must be deposited by a low-temperature process, such as the plasma-enhanced chemical vapor deposition (PE–CVD) method [11]. In particular, for waveguides associated with electronic structure, it is essential to use a low-temperature process so as not to damage the electronic devices.

Figure 1.10a shows a scanning electron microscope (SEM) image of the core of a silicon photonic wire waveguide with a cross-section of $400 \times 200\,\mathrm{nm}^2$ [8]. The geometrical shape closely matches the design values, and the perpendicularity of the sidewalls is also very good. Figure 1.10b shows a photograph of the 80-nm-wide

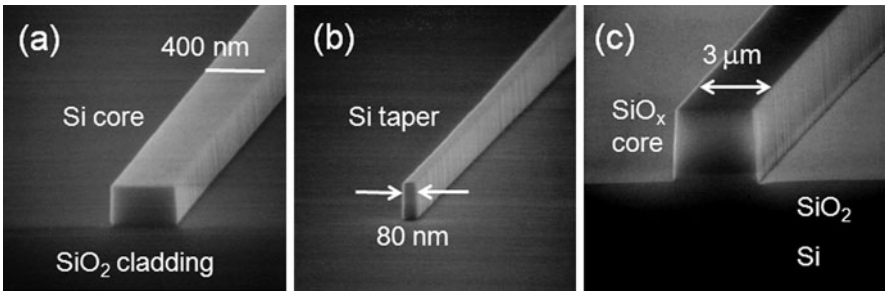

Fig. 1.10 SEM images of a silicon photonic wire waveguide system. (**a**) Core of silicon photonic wire waveguide, (**b**) silicon taper, and (**c**) core of SiOx waveguide for spot size converter

taper tip in the SSC. The taper and waveguide core were constructed by using a common fabrication process. Figure 1.10c shows an SEM photograph of the core of the silica waveguide for the SSC. The silica waveguide core was fabricated by depositing SiO_2-based material by the PE–CVD method and etched by reactive ion etching (RIE). By adjusting the deposition conditions, the refractive index of the material is tuned to be 2.5% higher than that of an ordinary thermal oxide. In the final product, a 7-μm SiO_2 overcladding layer covers the whole structure.

1.3.2 Propagation Performance

Figure 1.11 shows a typical transmission loss of silicon photonic wire waveguides with SSC, fabricated in the manner mentioned above. High-NA optical fibers with 4.3-μm mode field diameter (MFD) are used for external coupling. As shown in this figure, the propagation loss for the TE-like mode has been improved to be around 1 dB/cm. In the waveguide with flat cores, the propagation losses for TM-like modes are generally better than those for TE-like modes. Oxidation of the core sidewalls may further reduce the propagation losses [24]. The propagation loss of around 1 dB/cm is already at a practical level, since photonic devices based on silicon photonic wire waveguides are typically smaller than 1 mm. Besides the sidewall

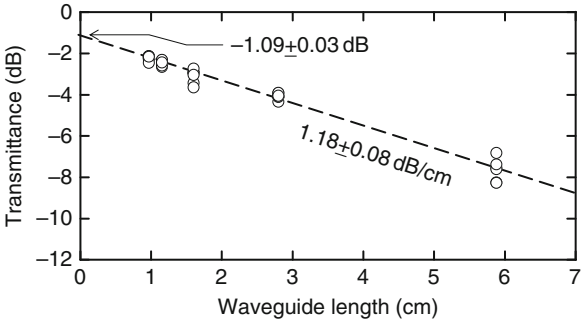

Fig. 1.11 Measured propagation loss of a silicon photonic wire waveguide with spot size converters

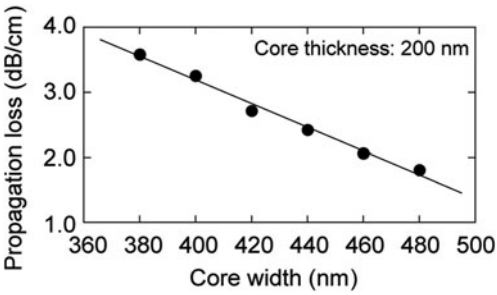

Fig. 1.12 Relation between measured propagation losses and core width

roughness of the core, the core width affects propagation losses as well. Figure 1.12 shows the relation between measured propagation losses and core widths. As shown, the propagation loss is reduced by increasing the core width because the effect of sidewall roughness is reduced in a wide core. When the core width exceeds 460 nm, the waveguide can also guide a higher order mode which may degrade the performances of some photonic devices.

The coupling loss between optical fiber and silicon photonic wire waveguide is represented by the intercept of the vertical axis in Fig. 1.11. The loss value at the intercept includes two waveguide/fiber interfaces; therefore in this case, one interface has a 0.5 dB coupling loss at a wavelength of 1,550 nm.

Figure 1.13 shows the transmission spectrum of a silicon photonic wire waveguide with SSCs. The spectrum remains flat over a 200-nm wide bandwidth, and no absorption dip is observed. The flat spectrum means that the SiO_2-based material used in the SSC does not contain impurities with N–H bonds. Although absorption by residual O–H bonds exists at wavelengths of around 1,400 nm, the resulting losses are not large. It is also possible to eliminate O–H bonds by heat treatment.

Figure 1.14 shows bending losses of single mode waveguides for TE-like modes. For the bending radius of over 5 μm, bending losses are negligible. Even for an ultra-small bending radius of around 2 μm, a waveguide with a flat core maintains

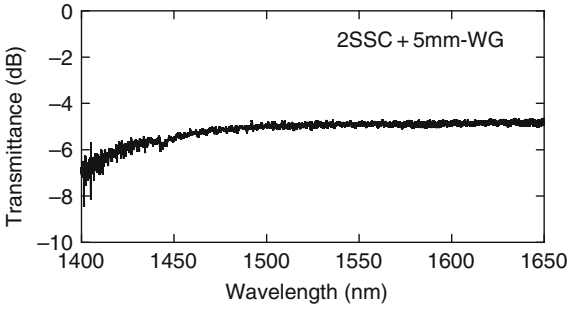

Fig. 1.13 Measured transmission spectrum of a typical silicon photonic wire waveguide with spot size converters

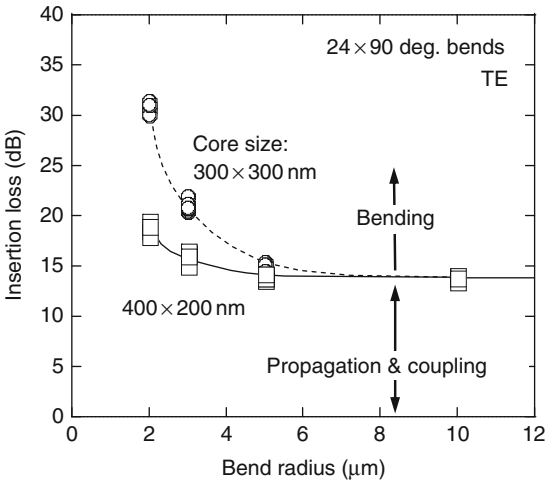

Fig. 1.14 Relation between measured insertion losses of the waveguides and bending radius

a low loss of below 0.1 dB per 90° bend. A waveguide with a square core shows a larger bending loss for a bending radius below 5 μm. For TM-like modes, especially in waveguides with flat cores, bending losses are generally larger than those for TE-like modes. Bending losses measured in various research groups are summarized in [10].

The birefringence of the waveguide can be evaluated by the free spectral ranges (FSRs) of ring resonators. Figure 1.15 shows measured transmission spectra at around 197 THz ($\lambda = 1.514\,\mu$m) for a ring resonator of 10-μm radius. In this figure, the FSR in TM-like modes (1.67 THz) is significantly larger than that in TE-like modes (1.11 THz). Using the FSR, we can roughly express the group index of the waveguide by $n_g = c/2\pi R\Delta f$, where c, R, and Δf are the speed of light in a vacuum, the radius of the ring resonator, and the FSR in hertz, respectively. Thus, the group indices are estimated to be 4.30 and 2.86 for TE and TM modes, respectively, which agree well with the design values in the previous section.

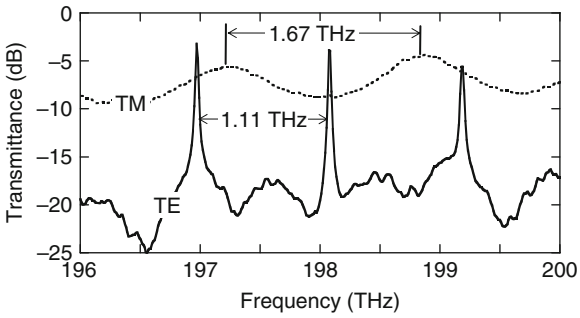

Fig. 1.15 Measured drop port spectra of a ring resonator with 10-mm radius

1.4 Simple Applications of Silicon Photonic Wire Waveguides

1.4.1 Passive Devices

The simplest passive device is a branch. Various branching devices, such as a Y branch and a multimode interference (MMI) branch, have been proposed and fabricated with silicon-wire waveguides [6, 7]. Figure 1.16a shows a multi-stage branch implemented with MMI branches [25]. The MMI branch units are no more than 3 μm in size, and the waveguides can bend light with a micrometer radius, so it is easy to configure multi-stage branches in a small area. Figure 1.16b shows the transmittance of the cascaded MMI branches for each output port. The transmittance linearly decreases with respect to the branching order. In other words, the branches of each stage are fabricated with uniform quality.

Compact add/drop wavelength filters are also being developed by using the ultra-compact bending parts of silicon-wire waveguides. Various ring-resonator-based filters have been developed. A single resonator is very compact and suitable for high-density integration; however, its Lorentzian resonance, as shown in Fig. 1.15, is not suitable for filters for telecommunications applications, which require flat pass bands. For a flat pass band, cascaded ring resonators have recently been developed [26].

Complex wavelength filters, such AWG filters [16, 27] and the lattice filters [28, 29], have also been developed. A photograph of a lattice filter is shown in Fig. 1.17a. In such filters, the pass-band spectrum can be fine-tuned by applying various optimization techniques, such as apodization. As shown in Fig. 1.17b, for

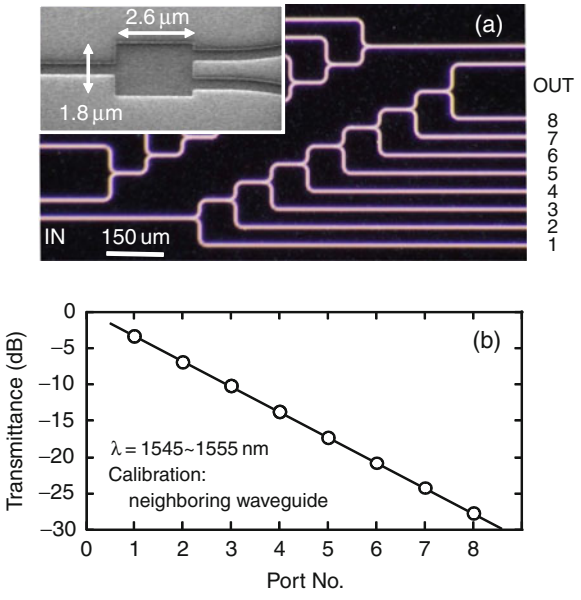

Fig. 1.16 (**a**) Cascaded MMI branches and (**b**) their transmission characteristics